

# High- and Low-Mass Star Forming Regions from Hierarchical Gravitational Fragmentation. High local Star Formation Rates with Low Global Efficiencies

Enrique Vázquez-Semadeni<sup>1</sup>, Gilberto C. Gómez<sup>1</sup>, A.-Katharina Jappsen<sup>2</sup>, Javier Ballesteros-Paredes<sup>1</sup> and Ralf S. Klessen<sup>3</sup>

Received \_\_\_\_\_; accepted \_\_\_\_\_

Submitted to ApJ

---

<sup>1</sup>Centro de Radioastronomía y Astrofísica, Universidad Nacional Autónoma de México, Apdo. Postal 3-72, Morelia, Michoacán, 58089, México

<sup>2</sup>School of Physics & Astronomy, Cardiff University, Queens Buildings, The Parade, Cardiff CF24 3AA, UK

<sup>3</sup>Zentrum für Astronomie der Universität Heidelberg, Institut für Theoretische Astrophysik, 69120 Heidelberg, Germany

## ABSTRACT

We investigate the properties of “star forming regions” in a previously published numerical simulation of molecular cloud formation out of compressive motions in the warm neutral atomic interstellar medium, neglecting magnetic fields and stellar feedback. We study the properties (density, total gas+stars mass, stellar mass, velocity dispersion, and star formation rate) of the cloud hosting the first local, isolated “star formation” event and compare them with those of the cloud formed by the central, global collapse event. In this simulation, the velocity dispersions at all scales are caused primarily by infall motions rather than by random turbulence. We suggest that the small-scale isolated collapses may be representative of low- to intermediate-mass star-forming regions, with gas masses ( $M_{\text{gas}}$ ) of hundreds of solar masses, velocity dispersions  $\sigma_v \sim 0.7 \text{ km s}^{-1}$ , and star formation rates (SFRs)  $\sim 3 \times 10^{-5} M_{\odot} \text{ yr}^{-1}$ , while the large-scale, massive ones may be representative of massive star forming regions, with  $M_{\text{gas}}$  of thousands of solar masses,  $\sigma_v \sim$  a few  $\text{ km s}^{-1}$ , and SFRs  $\sim 3 \times 10^{-4} M_{\odot} \text{ yr}^{-1}$ . We also compare the statistical distributions of the physical properties of the dense cores appearing in the central region of massive collapse with those from a recent survey of the massive star forming region in the Cygnus X molecular cloud, finding that the observed and simulated distributions are in general very similar.

However, we find that the star formation efficiency per free-fall time ( $\text{SFE}_{\text{ff}}$ ) of the high mass region, similarly to that of OMC-1, is low,  $\sim 0.04$ . In the simulated cloud, this is *not* a consequence of a “slow” SFR in a nearly hydrostatic cloud supported by turbulence, but rather of the region accreting mass at a high rate. Thus, we find that measuring a low  $\text{SFE}_{\text{ff}}$  may be incorrectly interpreted as implying a lifetime much longer than the core’s local free-fall time, and an SFR

much slower than that given by the free-fall rate, if the accretion is not accounted for. We suggest that, rather than requiring a low value of the  $SFE_{\text{ff}}$  everywhere in the Galaxy, attaining a globally low specific SFR requires star formation to be a spatially intermittent process, so that most of the mass in a GMC is not participating of the SF process at any given time. Locally, the specific SFR of a star-forming region can be much larger than the global GMC's average.

*Subject headings:* ISM: clouds — ISM: evolution — Stars: formation

## 1. Introduction

The formation of massive stars is currently a matter of intense debate (e.g., Zinnecker & Yorke 2007). High-mass star forming regions are characterized by more extreme physical conditions than their low-mass counterparts, containing cores of size, mass, and velocity dispersion roughly an order of magnitude larger than those of cores in low-mass regions (e.g. Jijina, Myers & Adams 1999; Lee & Myers 1999; Garay & Lizano 1999; Kurtz et al. 2000; Beuther et al. 2007). In particular, typical values of the properties of clumps within high-mass star forming regions (HMRs) are sizes 0.2–0.5 pc, mean densities  $n \sim 10^5 \text{ cm}^{-3}$ , masses between 100 and 1000  $M_{\odot}$ , and velocity dispersions ranging between 1.5 and 4  $\text{km s}^{-1}$ . In turn, the clumps break down into even denser “cores” that are believed to be the immediate precursors of single or gravitationally bound multiple massive protostars.

The high velocity dispersions of clumps in HMRs are generally interpreted as strong turbulence that manages to support the clumps against gravity (e.g., Garay & Lizano 1999; McKee & Tan 2003). However, the notion of “turbulent support” is difficult to maintain at the scales of these cores. If turbulence is to “support” a cloud against self-gravity, it must consist of isotropic motions, with typical scales significantly smaller than the size of the cloud, so that collectively these motions can act as a source of isotropic pressure, similarly to thermal molecular motions (Mac Low & Klessen 2004; Ballesteros-Paredes et al. 2007).

However, turbulence is a flow regime in which the largest velocity differences are associated with the largest separations (e.g. Frisch 1995), so that, in a turbulence-induced density fluctuation (i.e., a cloud or clump), the largest velocity difference is expected to occur at scales comparable to the size of the clump itself, thus being *highly anisotropic* with respect to it. This property is indeed observed in molecular clouds, in which a principal component analysis of the velocity structure shows that the dominant mode is dipole-like

(Heyer & Brunt 2007), indicating either shear or compression, but not solid-body rotation (M. Heyer, 2009, private communication). Being dipolar, the principal velocity component appears unsuited to act as a supporting form of pressure capable of opposing self-gravity.

Moreover, in the case of supersonic turbulence, the clumps are expected to be formed by large-scale compressive motions (Hunter & Fleck 1982; Ballesteros-Paredes et al. 1999a, 2003; Klessen et al. 2005), suggesting that the turbulence *within the clumps* is similarly likely to have a strong compressive component. Indeed, Vázquez-Semadeni et al. (2008) presented a numerical study of turbulent clouds driving showing that, even with continuous *random* driving at large scales, there is a trend for the clumps to contain a net convergence of the flow. This result contradicts the hypothesis that the non-thermal motions consist of isotropic, small-scale turbulence. After all, the clumps *must* be formed by a globally converging flow, as dictated by the continuity equation.

In addition, numerical simulations of cloud formation in the diffuse atomic ISM (e.g. Vázquez-Semadeni et al. 1995, 1996; Passot et al. 1995; Ballesteros-Paredes et al. 1999a,b; Koyama & Inutsuka 2002; Audit & Hennebelle 2005; Heitsch et al. 2005, 2006, 2008; Vázquez-Semadeni et al. 2006, 2007; Hennebelle & Audit 2007) and of star formation in turbulent, self-gravitating clouds (e.g. Klessen, Heitsch & Mac Low 2000; Heitsch, Mac Low & Klessen 2001; Klessen 2001; Bate, Bonnell, & Bromm 2003; Vázquez-Semadeni et al. 2005; Jappsen et al. 2005; Vázquez-Semadeni et al. 2007; Federrath et al. 2008, 2009) show that the velocity fields are in general organized at all scales, exhibiting a continuity from the large scales outside the clumps all the way to their interiors. Specifically, the simulations of molecular cloud formation by Vázquez-Semadeni et al. (2007, hereafter Paper I), showed that, as the cloud’s mass is consumed by the formation of collapsed objects (“stars”), the cloud continues to accrete mass from its surrounding, more diffuse (“atomic”) environment, the whole process

amounting to a “mass cascade”, analogous to a turbulent energy cascade, as proposed by Newman & Wasserman (1990) and Field, Blackman, & Keto (2008). Observational evidence supporting this scenario has been recently provided by Galván-Madrid et al. (2009).

In this paper, we investigate the consequences of this hierarchical fragmentation scenario on the formation of low- and high-mass star forming regions, taking advantage of the variety of star forming regions appearing in the main simulation of Paper I. This study was motivated by a careful observation of the mechanism through which the clouds are assembled in that simulation. Specifically, we show that the region in the simulation with physical conditions resembling those of observed massive star-forming regions forms as the result of the large-scale collapse of a large complex, thus suggesting that such regions may be in generalized gravitational collapse rather than in a quasi-static state supported by turbulence, as proposed, for example, by Hartmann & Burkert (2007) for the Orion molecular cloud.

The plan of the paper is as follows. In §2 we briefly recall the main parameters and evolutionary features of the numerical simulation, and identify the regions we investigate. In §3 we measure the evolution of the total (dense gas + “stars”) and “stellar” masses, and the instantaneous star formation rate (SFR) in both the isolated, peripheral, low-mass region (LMR) and in the central, global-collapse HMR. In §4 we then compare our results with available observations. In §4.1 we compare the physical conditions and the star formation rates, showing that these indicators are reasonably similar to those of actual star forming regions of each type. Next, in §4.2 we perform a survey of the cores in our HMR, and compare the distributions of their sizes, masses and densities with those of a recent survey of the Cygnus X region by Motte et al. (2007), showing that the distributions are very similar. Finally, in §6 we discuss the limitations of our study and present a summary.

## 2. The numerical model

### 2.1. Parameters

In this paper, we analyze data from the simulation labeled L256 $\Delta v$ 0.17 in Paper I. We refer the reader to that paper for details. Here we just mention that it is a smoothed particle hydrodynamics (SPH) simulation, performed with the GADGET code (Springel et al. 2001), including self-gravity and parameterized heating and cooling that imply a thermally bistable medium. The simulation uses  $3.24 \times 10^6$  SPH particles, and uses the prescription by Jappsen et al. (2005) for forming “sink particles” at densities above a certain density threshold, which we take as  $n_{\text{thr}} = 3.2 \times 10^6 \text{ cm}^{-3}$ . Once formed, the sinks can continue to accrete mass from their surroundings. Note, however, that the sinks are not sufficiently resolved in mass to be considered individual stars, and should be considered stellar clusters instead. The total mass in the simulation is  $5.26 \times 10^5 M_{\odot}$ , the size of the numerical box is 256 pc, and the initial conditions are uniform, with  $T = 5000$  K and a mean density of  $n = 1 \text{ cm}^{-3}$ , in which two cylindrical flows are set up to collide at the center of the simulation. The flows have the same density and temperature as the rest of the box, but oppositely directed velocities of  $7.536 \text{ km s}^{-1}$ , corresponding to a Mach number of 1.22. The flows have a length of 112 pc and a radius of 36 pc.

It is worth noting that the cylindrical inflows are much narrower than the length of the numerical box, having a diameter of only 1/4 of the box length. This allows for interaction between the cloud and its environment, and also frees the cloud from boundary effects. Also, the length of the inflows is slightly shorter than the box length, so that the inflows are entirely contained within the box. This is because the boundaries are periodic, and thus the inflows cannot enter from the outside. This implies also that the total mass in the box is fixed.

## 2.2. Evolution

The simulation we consider in this paper was designed to represent the formation and initial evolution of a dense, cold cloud out of the collision of streams of warm neutral gas. The collision nonlinearly triggers a phase transition to the cold neutral phase (Hennebelle & Pérault 1999; Walder & Folini 2000; Koyama & Inutsuka 2002; Heitsch et al. 2005; Audit & Hennebelle 2005; Heitsch et al. 2006; Vázquez-Semadeni et al. 2006, 2007; Hennebelle & Audit 2007), forming a large, flattened, and cold atomic cloud, which is turbulent because of a variety of instabilities in the interface between the cold and warm components (Koyama & Inutsuka 2002; Heitsch et al. 2006; Vázquez-Semadeni et al. 2006). The turbulence is moderately supersonic with respect to the cold gas.

Because the cloud is colder and denser, it readily becomes self-gravitating and begins contracting and fragmenting, so that the large atomic cloud becomes a large molecular-like cloud complex. The densest fragments begin to undergo small-scale, local collapse events (Banerjee et al. 2009). These isolated collapse events occur in a peripheral ring, which forms because the collapse of a finite sheet-like cloud proceeds from the outside in, as shown by Burkert & Hartmann (2004). Also, the local collapses occur *before* the bulk of the cloud completes its global, large-scale collapse, and the clumps and the stars they form are part of the global collapse of the complex. In the remainder of the paper, we show that the site at which the global collapse finally converges has physical conditions very similar to those of HMRs, while a typical local-collapse region has physical conditions resembling those of LMRs.

The large atomic cloud formed by the flow collision, which later becomes a denser “molecular cloud”<sup>1</sup> complex permeated by an atomic substrate, has a flattened shape

---

<sup>1</sup>The simulation does not follow the chemistry, but we refer to gas with density and

during most of its evolution. The large-scale gravitational contraction begins at  $t \sim 10$  Myr, and star formation begins at  $t \sim 17$  Myr. The initial radius of the peripheral ring is  $\sim 20$  pc. By  $t = 23.4$  Myr, the global collapse is completed (the ring has shrunk to nearly zero radius), although the turbulence in the cloud has caused the infall motions to have a random component, so that the collapse center spans several parsecs across. Animations showing the large-scale evolution of this simulation can be found in the electronic edition of Paper I.

It is important to note that in Paper I we applied a prescription by Franco, Shore & Tenorio-Tagle (1994) to estimate *a posteriori* the time at which the total stellar mass formed in the simulation would imply the presence of enough massive stars to reionize the whole complex. We found this time to be roughly 3 Myr after the onset of star formation, or roughly at  $t \sim 20$  Myr. However, simulations including ionization-heating feedback (Vázquez-Semadeni, Colín & Gómez, in prep.) suggest that, while the feedback is capable of disrupting the small-scale clumps, it does not prevent the large-scale collapse to form the massive region, since the material that falls into the latter comes from much larger distances than the local spheres of influence of the stellar sources (see also Dale et al. 2005; Dale & Bonnell 2008; Peters et al. 2009). In addition, the cloud continues accreting mass from the warm medium even while it is actively forming stars. Thus, it is safe to assume that the central massive region would form even if we had included stellar feedback in the present simulation.

---

temperature typical of molecular gas as “molecular”.

### 2.3. The regions

In this paper, we focus on two different regions of “star” (i.e., sink particle) formation. As a representative example of an LMR, we consider the first region to ever form stars in the peripheral ring starting at  $t = 17.3$  Myr, which involves relatively small mass in both gas and sinks. Other LMRs in the simulation are similar to this one. As an example of an HMR, we consider the central region, where the global collapse converges at  $t = 23.4$  Myr. We choose this time because it is the time of maximum compression of the material (see the animations corresponding to Fig. 2 in the electronic edition). This region involves a substantially larger amount of mass than the LMR, and is the only such region formed in the simulation, because the total mass in the complex is only  $\sim 5 \times 10^4 M_{\odot}$  at the time we explore this region. Thus, this is our only choice for this type of region. Presumably, a more massive simulation could form a larger number of such regions.

Figure 1 shows a column density map of the LMR at  $t = 19.1$  Myr. The image is integrated over 16 pc in the  $x$ -direction. In the electronic version of the paper, this figure corresponds to an animation showing the evolution of this region from  $t = 16.6$  to 19.9 Myr. The dots show the newly formed sink particles. Figure 2 shows images of the central 8 parsecs of the simulation (the HMR), at  $t = 24.2$  Myr, viewed edge-on (*left*) and face-on (*right*). In the electronic version, this figure shows animations of the same region from  $t = 22.6$  to 25.2 Myr for both views. In the images and animations of Fig. 2 we do not show the sink particles because a large number of previously formed particles is already present in the region, and it is not easy to see the particles formed there.

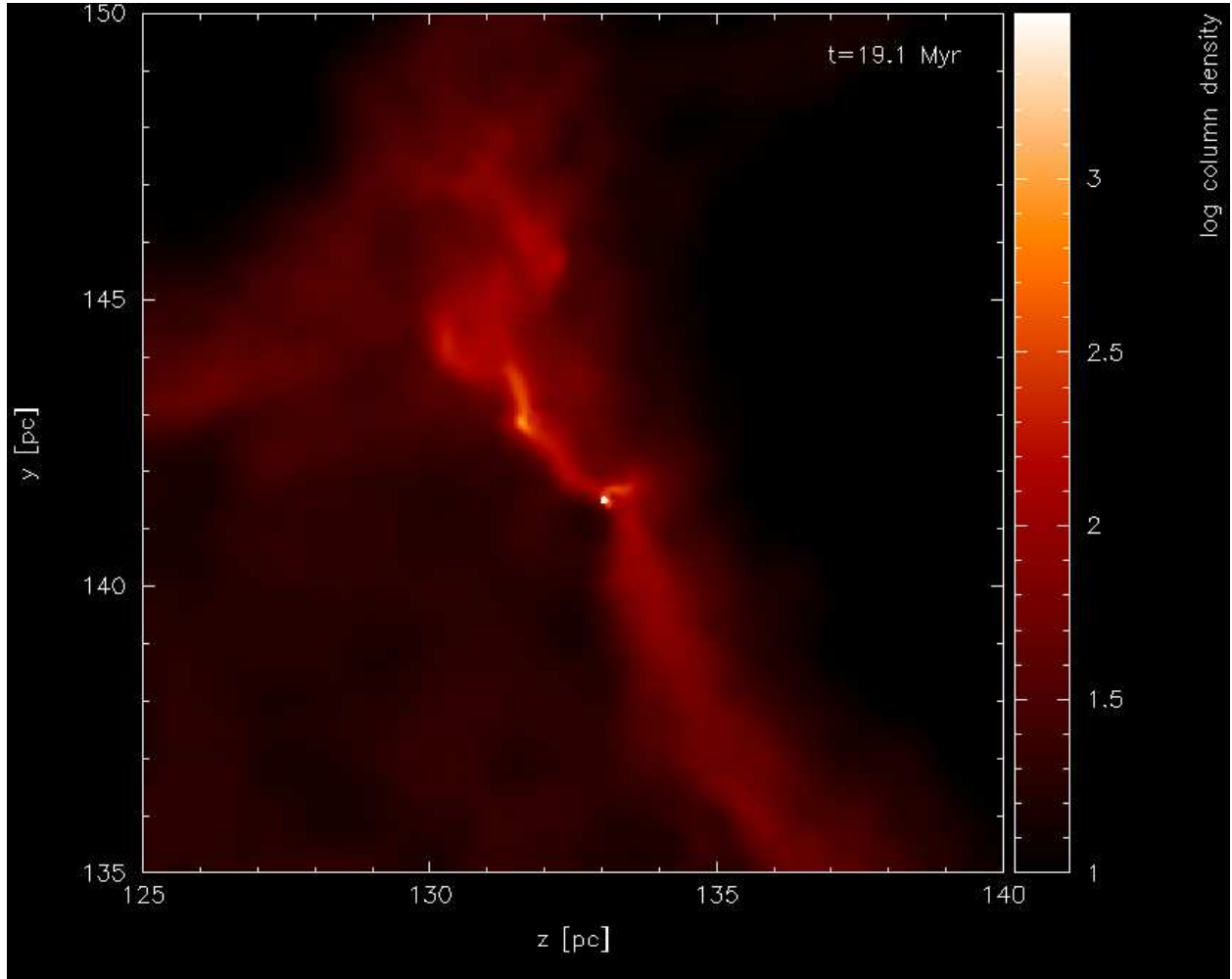


Fig. 1.— Column density plot of Cloud 1 in the  $y$ - $z$  plane at  $t = 19.1$  Myr, integrating over the central 16 pc along the  $x$  direction. The dots show the stellar objects (sink particles). The electronic version of this figure shows an animation of this region from  $t = 16.6$  to 19.9 Myr. The column density is in code units, which correspond to  $9.85 \times 10^{19} \text{ cm}^{-2}$ .

### 3. Physical conditions of the “low”- and “high”-mass regions

We begin our comparison study between the two regions by measuring the evolution of physical and star-forming properties of the “clouds” in these regions. To this end, we interpolate the SPH data of the regions shown in Figs. 1 and 2 onto a  $256^3$  grid in order to manipulate the data with the IDL software. We then define the clouds as connected sets of pixels with densities above  $n_{\text{th}} = 500 \text{ cm}^{-3}$ . We refer to the resulting clouds as “Cloud 1” (C1) in the LMR, and “the Central Cloud” (CC) in the HMR. In Fig. 3 we compare the evolution of the physical properties of the two clouds over a few Myr. Note that the starting times ( $t_0$ ) for the evolutionary plots are different in the two cases, being  $t_0 = 17.27$  Myr for C1 and  $t_0 = 22.58$  Myr for the CC. The *thick lines* correspond to the CC, and the *thin lines* correspond to C1. The *left column* shows the evolution of the density, size and velocity dispersion for the two clouds, where the size is calculated as  $r = (3V/4\pi)^{1/3}$ ,  $V$  being the volume of the cloud.

From these figures we see that the CC clearly has larger density, size, velocity dispersion, and mass than C1, at least during the time spans shown in the figures (C1 later acquires more mass and becomes more similar to the CC). Although the density of the CC is only a factor of 2 larger than that of C1 on average, we see that its size ranges between half and one order of magnitude larger than that of C1, and similarly for its velocity dispersion, which is on the order of a few  $\text{km s}^{-1}$ , as is the case for HMRs (e.g., Beuther et al. 2007). Similarly, the CC’s mass ranges in the thousands of solar masses, while that of C1 initially ranges in the hundreds, although, as mentioned above, this region is growing in time, and approaching the conditions of the CC at late times. Note that the gas mass in the CC is initially less than the sink mass because we include the mass of pre-existing sinks in the region, and not only the sinks formed by the CC. We do this because we next compute with the virial mass of the system, which must be compared with the total gravitational mass,

including the gas and all sinks in the region.

We compute the virial mass of each region applying the standard formula

$$M_{\text{vir}} \equiv 210 \left( \frac{R}{\text{pc}} \right) \left( \frac{\Delta v_{\text{eff}}}{\text{km s}^{-1}} \right)^2 M_{\odot}. \quad (1)$$

(see, e.g., Caselli et al. 2002; Tachihara et al. 2002; Klessen et al. 2005). It is noteworthy that the CC, even though it is in an extremely dynamic infalling state, has a ratio of mass to virial mass  $M/M_J$  of almost exactly unity during most of its evolution. This is precisely what is expected for an object undergoing gravitational contraction, and has been observed previously in numerical simulations (e.g., Klessen & Burkert 2000, 2001; Vázquez-Semadeni et al. 2007). Instead, this ratio is completely arbitrary in the case of clouds or clumps formed purely by turbulent compressions.

Cloud 1, on the other hand, starts with a ratio of nearly 5, but it steadily approaches unity as it accelerates in its contraction. Note that such values of this ratio are not uncommon in observed low-mass clouds (see, e.g., Tachihara et al. 2002; Morata et al. 2005). Presumably, the relatively large initial values of the ratio indicate that at its initial states, the cloud is only beginning to decouple from the global flow, and starting its own collapse.

We furthermore measure the *sink* formation rate (SiFR) in both clouds, defined as

$$\text{SiFR} = \frac{\Delta M_{\text{sink}}}{\Delta t}, \quad (2)$$

where  $\Delta M_{\text{sink}}$  is the increment in sink mass in the region during the time interval  $\Delta t = 0.13$  Myr between successive data dumps. Analogously, we define the “specific SiFR” (*sifr*) as

$$\text{sifr} = \frac{\text{SiFR}}{M_{\text{gas}}}, \quad (3)$$

where  $M_{\text{gas}}$  is the instantaneous dense gas mass in the region, again defined as the mass of gas with densities  $n > 500 \text{ cm}^{-3}$ . Note that, for simplicity, we perform these measurements

directly on the SPH data, rather than on their interpolation on a grid. Note also that we use the increment in the mass of the sinks rather than in the number of sinks because, as mentioned in §2, our sinks are not sufficiently resolved in mass, and furthermore they continue to accrete mass after they form, as shown in Fig. 4. This figure shows the mass evolution of the most massive sinks formed in the simulation up to  $t = 20$  Myr (*left panel*), the most massive sinks formed in the central 8-pc region for  $23.9 < t < 25$  Myr (*middle panel*), and those formed outside of the central 8-pc region during the same time interval (*right panel*).

Both the SiFR and the *sifr* are shown in Fig. 5. It is clearly seen that again the SiFR of the CC is roughly one order of magnitude larger than that of C1. However, it is seen that the *specific* star formation rate is similar for both clouds, suggesting that the larger SiFR of the CC is due exclusively to the larger amount of mass available for collapse in this cloud. In any case, if one assumes a universal IMF, then the larger SiFR of the CC implies that it has a ten-fold larger likelihood of forming massive stars, in correspondence with its more massive and violent status.

#### 4. Comparison with observations

In this section we compare the mean physical properties of the massive clump in the CC with those of a typical massive-star forming clump in the Orion Molecular Cloud, namely the well-known clump OMC-1. Next we compare the statistical distributions of masses, sizes and densities of the dense cores in the Cygnus-X North region, reported by Motte et al. (2007) with the corresponding structures within the CC.

It is important to note that, since we are making these comparisons against data from two different molecular clouds, we are making the implicit assumption that the massive-star

forming clumps in GMCs are similar in different clouds, constituting a general class of objects. This is, however, a reasonable assumption, since these clumps are often discussed in general terms, regardless of the GMC to which they belong (see, e.g., the discussion in Beuther et al. 2007, sec. 2.1).

#### 4.1. Physical properties and star formation rates

We begin by considering a typical HMR, namely OMC-1, the gas behind the Orion Nebula Cluster (ONC) in the Orion Molecular Cloud (OMC). According to Bally et al. (1987), the total gas mass in the clump known as OMC-1 is  $\sim 2200 M_{\odot}$  and the typical observed (i.e., 1D) rms velocity is  $\sim 2 \text{ km s}^{-1}$ , with an angular size  $\Delta\theta \sim \sqrt{108}$  arcmin (see the first entry in their Table 1). Assuming a distance of 400–500 pc to OMC-1 (Genzel et al. 1981; Sandstrom et al. 2007), this value of  $\Delta\theta$  implies a physical size  $\sim 1.2$ – $1.5$  pc for this cloud. Thus, the mean density in OMC-1 is  $\sim 2200M_{\odot}/(1.35 \text{ pc})^3 \sim 900 M_{\odot}\text{pc}^{-3} \sim 1.54 \times 10^4 \text{ cm}^{-3}$ , where for the last term we have assumed a mean particle mass of 2.36.

The above numbers can be compared with the physical conditions in the CC in our simulation. To do this, we need to select the gas within this region with similar mean density. We have found that this is accomplished by using a density threshold of  $4500 \text{ cm}^{-3}$  to define the region, which gives us a mean density of precisely  $1.54 \times 10^4 \text{ cm}^{-3}$ .

Next, we apply a clump-finding algorithm based on identifying connected sets of grid points whose densities are above this threshold, allowing us to identify the most massive clump within the CC. This region can be considered the equivalent to what is often referred to as a “cluster-forming core” (Lada & Lada 2003). However, we refer to it as a “clump”. Once the clump is defined, we can straightforwardly measure its physical

properties. We find a gas mass  $M_{\text{gas}} \sim 3015 M_{\odot}$ , a size  $r \sim 1.14$  pc (computed through the formula  $r = (3V/4\pi)^{1/3}$ , where  $V$  is the volume of the clump), and a three-dimensional velocity dispersion  $\sigma \sim 4.74$  km s $^{-1}$ , implying a one-dimensional velocity dispersion of  $\sim 2.74$  km s $^{-1}$ . We thus find that there is very good agreement between the physical conditions in OMC-1 and those of an equivalent region within the CC in our simulation.

Moreover, from Fig. 5 we see that the CC is characterized by a SiFR  $\sim 10^{-3} M_{\odot} \text{ yr}^{-1}$  on average. Noting that our density threshold for the formation of a sink, of  $3.2 \times 10^6$  cm $^{-3}$ , is comparable to the density of a dense core, we should consider that the *star* formation efficiency (SFE) within our sinks is less than 100%. Assuming an SFE  $\sim 30$ –50%, we estimate a *star* formation rate (SFR)  $\sim 3$ – $5 \times 10^{-4} M_{\odot} \text{ yr}^{-1}$ . On the other hand, Tobin et al. (2009) report on 1613 stars in the ONC. Taking this number as a proxy for the total stellar production of this region, and a mean stellar mass of  $0.3 M_{\odot}$  (Hillenbrand & Carpenter 2000), this implies a total stellar mass of  $\sim 500 M_{\odot}$ . The estimated age spread of the cluster is  $\lesssim 2$  Myr (Hillenbrand 1997). We thus infer  $\text{SFR} \gtrsim 2.5 \times 10^{-4} M_{\odot} \text{ yr}^{-1}$ , in very good agreement with that of our CC.

With these data, we can also calculate the SFE per free-fall time,  $\text{SFE}_{\text{ff}}$ .<sup>2</sup> Specifically, writing

$$\text{SFE}_{\text{ff}} = \frac{M_{\text{stars}}(t_{\text{ff}})}{M_{\text{gas}} + M_{\text{stars}}(t_{\text{ff}})}, \quad (4)$$

where  $M_{\text{stars}}(t_{\text{ff}}) \approx \text{SFR} \times t_{\text{ff}}$ , with SFR being the instantaneous star formation rate, estimated above, and  $t_{\text{ff}}$  the free-fall time. At the mean density of  $1.54 \times 10^4$  cm $^{-3}$ , and a

---

<sup>2</sup>This quantity is frequently referred to as SFR per free-fall time in the literature. However, it is actually the *specific* SFR, integrated over a free-fall time (e.g. Krumholz & McKee 2005; Krumholz & Tan 2007).

temperature of 10 K, we have  $t_{\text{ff}} \approx 0.27$  Myr. We thus find

$$\text{SFE}_{\text{ff}} \approx \frac{135M_{\odot}}{3150M_{\odot}} = 0.043. \quad (5)$$

Interestingly, this value is fully consistent with that obtained by Krumholz & Tan (2007) ( $\text{SFE}_{\text{ff}} \sim 0.03\text{--}0.09$ ) for the ONC. We discuss this result further in §5.1.

Finally, we can also perform a comparison between the CC and OMC-1 at the level of the *core* formation rate. Ikeda et al. (2007) report a total mass of dense cores in the OMC-1 region of  $\sim 800 M_{\odot}$ . Assuming that these have typical lifetimes between 2 and  $5 \times 10^5$  yr (e.g., Hatchell et al. 2007), we find a core formation rate (CFR) between 1.6 and  $4 \times 10^3 M_{\odot} \text{Myr}^{-1}$ , which again compares very well to the mean value of the SiFR mentioned above. Note that the estimated CFR for OMC-1 is larger than the estimated SFR in the ONC by a factor of a few, a reasonable result if the efficiency of star formation within the cores is smaller than unity, and consistent with the factor we have used above for estimating the SFR from the SiRF.

We conclude that the physical conditions and SFR in a well-known massive-star forming clump agree to within less than factors of 2 with the corresponding features in the CC of our simulation.

## 4.2. Statistics of cores in the Central Cloud

As a further test of the similarity of the CC with massive-star forming clumps, in this section we compare the statistics of the dense cores within the CC with those reported by Motte et al. (2007) for the Cygnus X molecular complex. These authors have performed a 1.2 mm continuum unbiased survey of the massive-star forming clumps within the Cygnus-X complex, and reported the masses, sizes and densities of the cores within the clumps, and of the clumps themselves. Specifically, they compiled a large dataset of 129 massive

dense cores, of sizes  $\sim 0.1$  pc, masses  $M_{1.2 \text{ mm}} = 4\text{--}950 M_{\odot}$ , and densities  $n \sim 10^5 \text{ cm}^{-3}$ , listed in Table 1 of that paper. These data are very well suited for comparison with the corresponding structures in the CC of our simulation. In order to perform the comparison, we identify dense cores within the gridded version of the CC in our simulation (cf. Fig. 2) at time  $t = 23.9$  Myr, at which the global collapse of the entire cloud complex in the simulation is being completed (i.e., the clouds that had initially formed at the peripheral ring in the simulation reach the center at this time).

To define the cores, we apply the same clump-finding algorithm used in §4.1, but in this case we use it iteratively and with higher threshold densities to define an ensemble of cores. Specifically, we consider a set of four thresholds, at  $n = 10^4$ ,  $3 \times 10^4$ ,  $10^5$ , and  $3 \times 10^5 \text{ cm}^{-3}$ , and include all of the resulting data points into a single dataset. We do this in order to have a sufficiently large sample, and to allow for a wider dynamic range in the physical properties of the cores, since our previous experience shows that objects selected with a given threshold have mean densities that differ by less than an order of magnitude from the value of the threshold (e.g., Vázquez-Semadeni, Ballesteros-Paredes & Rodríguez 1997). Note that our procedure differs from other algorithms such as CLUMPFIND (Williams, de Geus & Blitz 1994) in that, in our case, clumps defined at a lower threshold may contain several clumps defined at a higher threshold, while CLUMPFIND, for example, does not identify such “parent” structures as a clump. We choose this procedure for simplicity, and because larger clumps defined at lower thresholds may be bound structures themselves that should be taken into account. Motte et al. (2007) themselves used a combination of source extraction analysis and GAUSSCLUMPS (Stutzki & Güsten 1990).

This procedure leaves us with 39 cores, 38 of which have  $M > 4M_{\odot}$ . For each core, we measure its mass, mean density, and velocity dispersion, and estimate its size as  $r \approx (3V/4\pi)^{1/3}$ , where  $V$  is its volume. The distributions of these properties can be

compared with those reported by Motte et al. (2007) for any of the regions within the Cygnus-X complex. As a representative example, we choose the data for the Cygnus-X North region, which contains 72 cores (see their Table 1). We show the distributions of core properties for the Cygnus-X North region in the histograms presented in Fig. 6 by the *dotted* lines. Superimposed on these histograms, the *solid* lines show the corresponding distributions for the 38 cores more massive than  $4M_{\odot}$  in the CC of our simulation. We see that the distributions match extremely well for size, mass, and mean density. No comparison is made for the velocity dispersions because Motte et al. (2007) do not report them, but in our sample, they range from  $\sim 0.2$  to  $\sim 3$  km s $^{-1}$ .

A final comparison that can be made is at the “clump” level. This is analogous to the comparison we made with OMC-1, but comparing against the mean properties of the clumps identified by Motte et al. (2007). They report the typical sizes, masses, and densities of all clumps to be  $r \sim 0.68$  pc,  $M \sim 1000M_{\odot}$ , and  $n \sim 1.4 \times 10^4$  cm $^{-3}$  respectively (see column 3 in their Table 4). Again, this is comparable to the clump we obtain thresholding our CC data at  $n_{\text{th}} = 4500$  cm $^{-3}$ , for which we find a mean density of  $n \approx 1.54 \times 10^4$  cm $^{-3}$ , a size  $r \approx 1.14$  pc, and a mass of  $3015 M_{\odot}$  (cf. §4.1). We see that our clump is somewhat more massive and extended than Motte et al. (2007)’s mean clump, but still within factors of 2–3 of the latter.

## 5. Discussion and caveats

### 5.1. The star formation efficiency per free-fall time

The results from §4.1 have a number of interesting implications. We note that the SF *rates* in both the CC in our simulation and in OMC-1 in Orion are relatively large,  $\sim 3 \times 10^{-4}M_{\odot}$  yr $^{-1}$ . This can be translated into a *specific* SFR (or inverse SF, or gas

depletion, timescale,  $t_{\text{SF}}^{-1}$ ), given by

$$t_{\text{SF}}^{-1} \approx \frac{\text{SFR}}{M_{\text{gas}} + M_*}, \quad (6)$$

where  $M_{\text{gas}}$  is the gas mass in the cloud and  $M_*$  is the stellar mass. We obtain  $t_{\text{SF}} \sim 10$  Myr for both the CC and OMC-1. This differs strongly from the much longer timescales  $t_{\text{SF}} \sim 2$  Gyr for extragalactic GMCs (Bigiel et al. 2008), and  $t_{\text{SF}} \sim 300$  Myr for Galactic GMCs (McKee & Williams 1997). Said another way, if one were to extrapolate (linearly with mass) the SFR of these clumps (the CC or OMC-1) to the entire molecular gas mass of the Galaxy of  $10^9 M_\odot$ , one would find a total Galactic SFR of  $\sim 3 \times 10^{-4} M_\odot \text{ yr}^{-1} \times 10^9 M_\odot / 3000 M_\odot = 100 M_\odot \text{ yr}^{-1}$ , or roughly 50–100 times larger than the observed SFR. This is the well known Zuckerman & Palmer (1974) conundrum. However, also in section §4.1, we showed that the  $\text{SFE}_{\text{ff}}$  of both regions is small, and fully consistent with the estimate of Krumholz & Tan (2007) for ONC, and the general result of a low  $\text{SFE}_{\text{ff}}$  for the cores in the survey by Evans et al. (2009).

These results then raise two important questions. The first is how to reconcile the much larger specific SFR of regions like the CC or OMC-1 with that of entire molecular clouds, or even the total molecular gas content of the Galaxy. The large disparity in  $t_{\text{SF}}^{-1}$  between individual cluster-forming clumps and large-scale objects like GMCs can be understood if star formation is a *spatially intermittent* phenomenon. That is, it does not occur everywhere in the molecular gas, but only at special locations, characterized by the highest densities. Thus, the small fraction of the mass that *is* forming stars must have a much larger specific SFR than the global average. This is analogous to the intermittency of the energy dissipation rate in incompressible turbulent flows, which is known to occur only at scattered locations, where the velocity gradient is maximized by vortex stretching (see, e.g., Frisch 1995).

The second question is: how can such an actively star forming region have such a small

value of the  $\text{SFE}_{\text{ff}}$ . The theory by Krumholz & McKee (2005) originally derived such low values for the  $\text{SFE}_{\text{ff}}$  for clumps in near virial equilibrium supported by turbulence (similarly to the underlying assumption of the model by McKee & Tan 2003). However, the CC in our simulation is far from being in equilibrium, as shown in the animations corresponding to Fig. 2.

The origin of the small  $\text{SFE}_{\text{ff}}$  value for the CC in our simulation can be understood by rewriting eq. (4) as

$$\text{SFE}_{\text{ff}} = \frac{\text{SFR}}{M_{\text{tot}}} t_{\text{ff}}, \quad (7)$$

where  $M_{\text{tot}}$  is the total mass (gas + stars) in the cloud. From this expression we see that a low value of the  $\text{SFE}_{\text{ff}}$  can be obtained through a large cloud mass and/or a high density (via  $t_{\text{ff}}$ ), besides the obvious possibility of a small SFR. This appears to be the case of the CC, which is rapidly increasing its mass through accretion of the surrounding gas at a rate that apparently overwhelms its consumption rate by SF. Indeed, Fig. 7 shows the evolution of the total gas mass in the central 8-pc box of the simulation in which the CC is contained. The gas mass is seen to increase from  $\sim 4000M_{\odot}$  to  $\sim 12000M_{\odot}$  in 3 Myr, corresponding to a mean accretion rate onto the region of  $\sim 2.7 \times 10^{-3}M_{\odot} \text{ yr}^{-1}$ , or roughly an order of magnitude larger than the SFR in the CC.

Moreover, because of the ram pressure (or, equivalently, weight) of the accreting material, the density is also larger than what would be expected if the clump were isolated and in hydrostatic equilibrium. That is, the actual collapse timescale of a region such as our CC and its surroundings is *longer* than the free-fall time of the central dense core alone, because the mean density of the combined system is lower than that of the core, and the material is continuously being replenished at the central regions. Thus, if the infalling material is unseen for any reason (e.g., thresholding, background subtraction, termination of the tracer excitation, etc.), then the central core will appear to have a shorter free-fall

time than the actual timescale of the collapse. This can be incorrectly interpreted as an isolated, equilibrium core with a lifetime much longer than its local free-fall time and thus with an SFR much slower than that given by the free-fall rate.

Finally, it is worth noting that this scenario then naturally explains the large final efficiencies of cluster-forming clumps ( $\sim 30\text{--}50\%$ ; e.g., Lada & Lada 2003), without having to invoke lifetimes for these clumps that are much larger than their free-fall times. Also, in this accreting scenario, we see that *a low local value of the  $SFE_{\text{ff}}$  does not guarantee a globally low SFR*. Our results show that a region can have a large SFR and still have a low  $SFE_{\text{ff}}$ . The attainment of a globally low SFR seems to require a highly scattered and intermittent occurrence of the star-forming regions.

## 5.2. Neglect of stellar feedback

The simulation we have analyzed in this paper neglects two important processes existing in real molecular clouds, namely stellar feedback and magnetic fields. Concerning the former, it is generally believed that it is a key mechanism in keeping a low final SFE in molecular clouds and their clumps. However, at present it is still unclear whether this self-regulation of SF occurs abruptly, after a brief period of a high SFR, dispersing the star-forming region and quenching SF altogether locally (the so-called “rapid SF” scenario; e.g., Whitworth 1979; Elmegreen 1983; Elmegreen 2000; Elmegreen 2007; Larson 1987; Franco, Shore & Tenorio-Tagle 1994; Hartmann, Ballesteros-Paredes, & Bergin 2001), or whether it occurs continuously over longer times, maintaining the region in a near-equilibrium state, allowing it to last for several free-fall times, while maintaining a low SFR (the so-called “slow SF” scenario; e.g. Krumholz & McKee 2005; Krumholz, Matzner & McKee 2006; Li & Nakamura 2006; Krumholz & Tan 2007).

The behavior of our simulation is consistent with the “rapid SF” scenario, in which a given region forms stars at a high rate over a short period of time and then their feedback disrupts the cloud, possibly assembling a new star forming region at a new location, through the “collect and collapse” mechanism (Elmegreen & Lada 1977; Elmegreen 2007). Since the large complex and its fragments in our simulation begin their gravitational contraction several Myr before the first star-forming collapse events occur (cf. §2.2), it is natural to expect that the initial stages of SF in each region will occur in a gravitationally contracting environment, and to be characterized by a large SFR, until enough stars have been formed that they can strongly affect, and possibly disrupt their parent clump (e.g., Elmegreen 1983; Larson 1987; Franco, Shore & Tenorio-Tagle 1994).

Under this scenario, our simulation and the star-forming regions formed within it represent the assembly and early star-forming epochs of a region, although their long-time star formation efficiencies are too large ( $\sim 60\text{--}70\%$  after  $\sim 10$  Myr; cf. Paper I) because they lack the subsequent disrupting effect of the stellar feedback on the clump in which the stars form, and so SF continues unimpeded in each region until the gas is exhausted. However, this is a shortcoming that is only expected to become important later into the evolution of each region, when the accumulated number of stars becomes large enough to exert a strong influence on the cloud. As mentioned in §2.2, in Paper I we applied a prescription by Franco, Shore & Tenorio-Tagle (1994) to estimate this time, which we found to be  $\sim 3$  Myr after the onset of SF, although new simulations including stellar feedback (Dale et al. 2005; Dale & Bonnell 2008; Peters et al. 2009, Vázquez-Semadeni et al., in prep.) suggest that the effect of feedback is more complicated than that, and should be applied clump by clump. But, in any case, our simulation should be accurate before the time of disruption by feedback, for each new star-forming region formed.

On the other hand, the evolution of our simulation is inconsistent with the “slow”

scenario of star formation (e.g., Krumholz & McKee 2005; Krumholz & Tan 2007), in which clouds are assumed to be maintained in quasi-static equilibrium by the turbulence injected by stellar sources, as modeled by Matzner (e.g., 2002); Krumholz, Matzner & McKee (e.g., 2006); Li & Nakamura (e.g., 2006). Our simulation, although incapable of following the stages in which SF interacts strongly with the infall process onto the clouds, suggests that they should be already contracting in general by the time they begin forming stars, rather than being in a quasi-hydrostatic state. Besides, the studies suggesting such a hydrostatic state have been performed either in closed numerical boxes or with simplified geometries, so that the disruption of the cloud by its stars has been made overly difficult. Moreover, it appears unlikely that the effect of the stellar energy injection, which occurs at small scales, can somehow organize itself to produce the large-scale, dipolar character of the principal velocity component in the clouds (Heyer & Brunt 2007). Simulations in which the cloud is embedded in its diffuse medium and in full three-dimensional geometry, such as the one utilized here, but including the effects of stellar feedback, are necessary to properly address the issue (Vázquez-Semadeni et al., in prep.)

Our results are consistent with recent suggestions, based on comparisons between simulations and observations, that molecular clouds (e.g., Hartmann & Burkert 2007) and clumps (e.g. Peretto, Hennebelle & André 2007) may be in a state of gravitational collapse. If confirmed, these suggestions point towards a return to the original suggestion by Goldreich & Kwan (1974) that the observed linewidths in molecular clouds are due primarily to gravitational contraction. This suggestion was dismissed by Zuckerman & Palmer (1974) through the argument that this would imply a much larger average star formation rate in the Galaxy than observed. However, in the scenario of rapid SF the instantaneously high rates of SF are not a problem, if the star-forming clumps are soon disrupted by the stellar feedback before their entire mass is consumed by SF.

### 5.3. Neglect of magnetic fields

Our simulation also neglects the influence of magnetic fields, and as such it should be considered as representative of the evolution of the supercritical parts of the clouds, which are the ones that can undergo global collapse. For these regions, the presence of weak but nonzero magnetic fields can retard the collapse (Heitsch, Mac Low & Klessen 2001; Ostriker, Stone & Gammie 2001; Vázquez-Semadeni et al. 2005). In any case, if other parts of the clouds are subcritical and are thus held up against their self-gravity by the magnetic field, then they must contribute only a small (or nearly null) fraction of the SF in the Galaxy (Elmegreen 2007), since it is known that most stars form in cluster-forming regions (Lada & Lada 2003), while a subcritical region is expected to be a site of isolated, low-mass star formation. Of course, if a large fraction of the cloud’s mass is supported by the field, then the global SFE for the cloud will certainly be decreased, but the supercritical regions will still be responsible for the majority of the SF activity of the cloud, and those parts should have similar SFEs as our simulation. Moreover, as discussed in §5.1, it is precisely this kind of structure that is necessary to have a large fraction of the molecular mass *not* participating in SF, while the remaining small fraction (a few percent; see, e.g., Kirk et al. 2006) can be essentially free-falling, and accounting for most of the SF in the GMC.

### 5.4. Clump properties

Although the CC has been shown to reproduce several features of massive-star forming clumps, it does also exhibit certain differences. Most notably, the total mass in the CC contains roughly twice the mass in sinks than in gas at  $t - t_0 = 0$  (cf. Fig. 3, upper right panel). This is contrary to the situation in the ONC-OMC-1 complex, where the gas mass is roughly 4 times larger than the stellar mass. The excess sinks in the CC are “stragglers”, which were formed earlier in the peripheral ring, but that have fallen into the large potential

well of the whole complex together with the gas. This suggests that the global collapse responsible for the formation of the CC is somewhat too focused, perhaps as a consequence of the extremely smooth initial conditions used in the simulation. Indeed, experimentation with more strongly fluctuating initial conditions in the velocity (Rosas-Guevara et al. 2009) shows that in this case the collapse is less focused, possibly causing the population of infalling sinks in the collapse center to be less numerous. Nevertheless, the presence of such infalling stars may explain the age spreads observed in regions of massive star formation (Palla & Stahler 1999; Faustini et al. 2009).

Note also that, due to the presence of the infalling sinks, it is possible for both the gas and sink mass in the upper right panel of Fig. 3 to decrease simultaneously. This is a consequence of the gas being consumed to form new sinks, but with the SiFR not being able to compensate for the departure of the infalling sinks which, contrary to the situation of the gas, simply pass through the region, while the gas shocks and stagnates there.

Finally, it is necessary to remark that the dense cores necessarily lie at the limit of the scales resolved by the simulation. Thus, the velocity dispersion within them is most certainly reduced by numerical diffusion. However, the fact that the gravitational contraction is hierarchical, and starts at the largest scales of our cloud, implies that the collapsing nature of the clumps cannot be an artifact of the numerical diffusion.

## 6. Summary and Conclusions

In this paper we have presented numerical evidence that the physical conditions in low- and high-mass star forming regions (“clouds”) can arise from hierarchical gravitational collapse. The former regions arise from small-scale fragments in the collapse (which however occur first, because they originate from local high-amplitude density fluctuations which

have a shorter free-fall time), while the latter may appear when the global, large-scale collapse is completed. The local collapse events do not exhaust the gas in their regions because a) the consumption time is relatively long,  $\sim 5$  Myr (cf. Fig. 5, *right panel*), and b) because the clouds continue to accrete mass from their atomic surroundings throughout their evolution. Thus, the isolated low-mass clouds eventually collide to form a high-mass complex. In this scenario, velocity dispersions are caused primarily by infall motions rather than random turbulence, but its hierarchical nature may explain why massive cores tend to have larger velocity dispersions than low-mass ones at the same size (see, e.g., Fig. 10 of Garay & Lizano 1999), since the former only begin contracting when they decouple from the global flow, while the latter have been accelerating in their contraction for a longer time.

The evidence we presented consisted of two parts. First, we analyzed the evolution of the physical properties (mass, mean density, size, velocity dispersion, and mass to virial mass ratio), as well as of the SFRs of two examples of the class of objects, which we called “Cloud 1” (C1) and “the Central Cloud” (CC). We noted that the latter, which forms as a consequence of the large-scale collapse of the cloud complex in the simulation, contains a clump with properties consistent with those of cluster-forming cores within GMCs, such as a gas mass  $M_{\text{gas}} \sim 3000M_{\odot}$ , a velocity dispersion  $\sigma_v$  of a few  $\text{km s}^{-1}$ , and a star formation rate  $\text{SFR} \sim 3 \times 10^{-4}M_{\odot}\text{yr}^{-1}$ , while C1 is more reminiscent of low- or intermediate-mass regions, with  $M_{\text{gas}} \sim 400M_{\odot}$ ,  $\sigma_v \sim 0.7 \text{ km s}^{-1}$  (during its initial stages, as it later becomes more massive), and  $\text{SFR} \sim 3 \times 10^{-5}M_{\odot}\text{yr}^{-1}$ .

Secondly, we performed a survey of the dense cores in the massive cloud (the central 8 parsecs of the simulation at the time the large-scale collapse converges there), and compared their statistical properties with those reported for the dense cores in the Cygnus X cloud complex by Motte et al. (2007), finding that the distributions of both samples match each other very well. At the slightly larger-scale, “clump” level, we also found good agreement

between the mean properties reported by those authors and the “clump” in that region. These results suggest that indeed the convergence of the global collapse is a good model of HMRs.

This scenario, however, has the implication that the mechanism responsible for the low global Galactic SFR may be the result of SF being a spatially intermittent process, so that most of the molecular gas mass is *not* forming stars at any given time in the Galaxy, while those regions that *are* forming stars do so at a very high rate — a rate that in fact accounts for most of the SF activity in GMCs and the Galaxy. This, in turn, implies that the global specific SFR of the molecular gas in the Galaxy does not extrapolate linearly with mass (as assumed by, for example, Krumholz & Tan 2007) to estimate the specific SFR of a single SF region.

Finally, we found, somewhat unexpectedly, that the massive-SF-like region in our simulation exhibits a low  $\text{SFE}_{\text{ff}}$  ( $\sim 4\%$ ), in spite of having a large SFR of  $\sim 3 \times 10^{-4} M_{\odot} \text{yr}^{-1}$ , and it being the site of the large-scale collapse of the cloud formed in the simulation, rather than a hydrostatic structure supported by turbulent pressure. We attribute this to the high density and large accretion rate occurring in this region as a consequence of the culmination of the large-scale collapse. In particular, the region accretes mass at an even higher rate than that at which it is forming stars, even though the latter rate is large. This physical scenario calls for a new class of theoretical models that take into account the sources and sinks for the mass of a molecular cloud.

We gratefully acknowledge the incisive and profound questions by an anonymous referee, which pushed us into a much deeper understanding of the phenomena described in this paper than we initially had. The numerical simulation was performed in the cluster at CRyA-UNAM acquired with CONACYT grants to E.V.-S. 36571-E and 47366-F. The animations were produced using the SPLASH visualization tool (Price 2007). We

thankfully acknowledge financial support from CONACYT grants 47366-F to E. V.-S. and 50402-F to G. C. G., UNAM-PAPIIT grant IN110409 to J. B.-P. A.-K.J. acknowledges support by the Human Resources and Mobility Programme of the European Community under contract MEIF-CT-2006-039569. R.S.K. acknowledges financial support from the German *Bundesministerium für Bildung und Forschung* via the ASTRONET project STAR FORMAT (grant 05A09VHA) and from the *Deutsche Forschungsgemeinschaft* (DFG) under grants no. KL 1358/1, KL 1358/4, KL 1359/5. R.S.K. furthermore is thankful for subsidies from a Frontier grant of Heidelberg University sponsored by the German Excellence Initiative and for support from the *Landesstiftung Baden-Württemberg* via their program International Collaboration II.

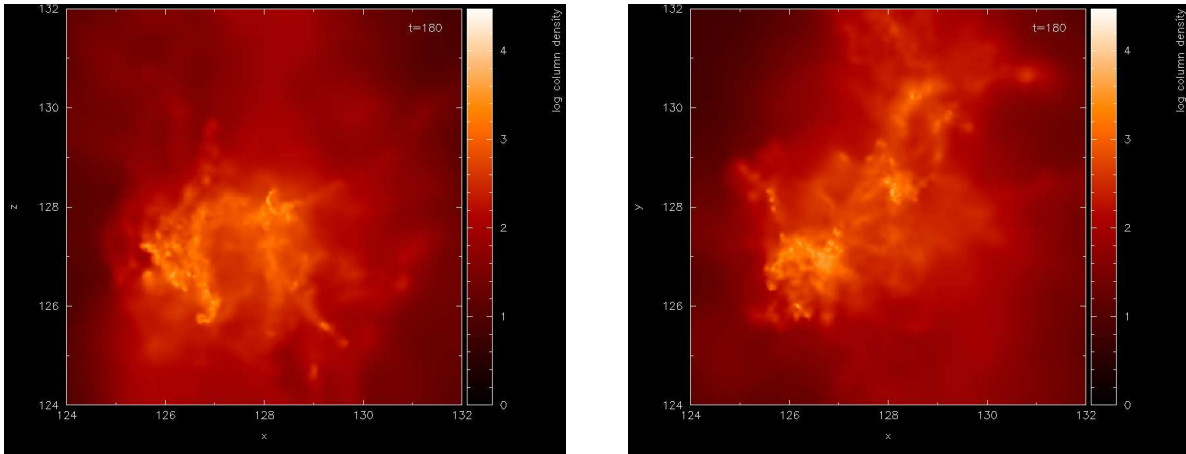


Fig. 2.— Two views of the central 8-pc cubic region. *Left panel:* Column density integrated along the  $y$  direction. *Right panel:* Column density integrated along the  $z$  direction. The electronic version of these images show the evolution of these regions from  $t = 22.6$  to  $25.2$  Myr.

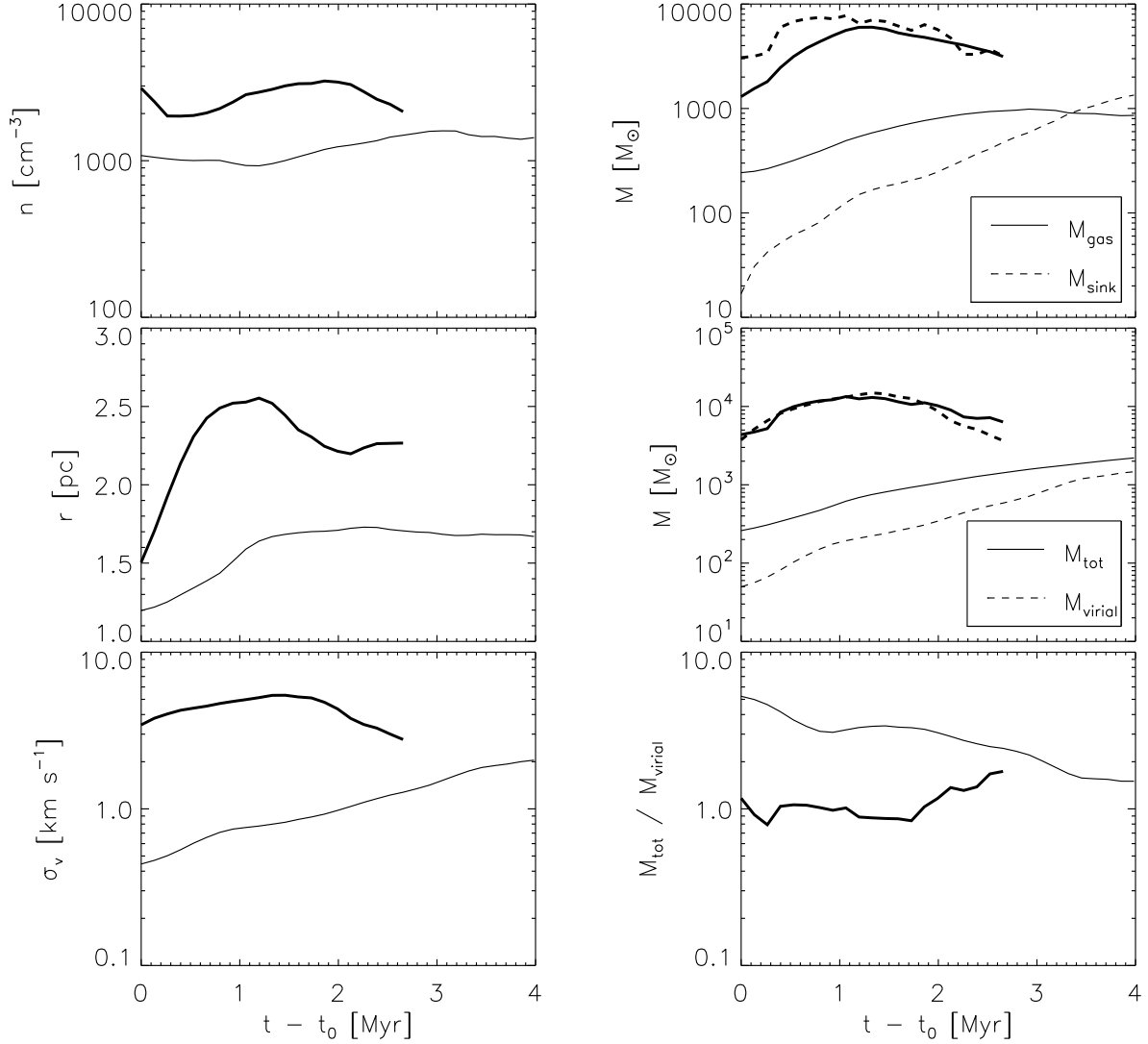


Fig. 3.— Evolution of the physical properties of the dense gas ( $n > n_{\text{th}} = 500 \text{ cm}^{-3}$ ) in the two star-forming regions analyzed in the simulation. The *thick lines* refer to the “Central Cloud” (CC), and the *thin lines* refer to “Cloud 1” (C1). *Left column*: Evolution of the mean density (*top panel*), size (*middle panel*), and velocity dispersion (*bottom panel*). *Right panel*: Evolution of the dense gas mass and sink mass (*top panel*); evolution of the total (dense gas+sinks) mass and the virial mass (*middle panel*); evolution of the ratio of total to virial mass (*bottom panel*). Note that the starting times  $t_0$  for the evolutionary plots are different for the two regions, being  $t_0 = 17.27 \text{ Myr}$  for C1 and  $t_0 = 22.58 \text{ Myr}$  for the CC.

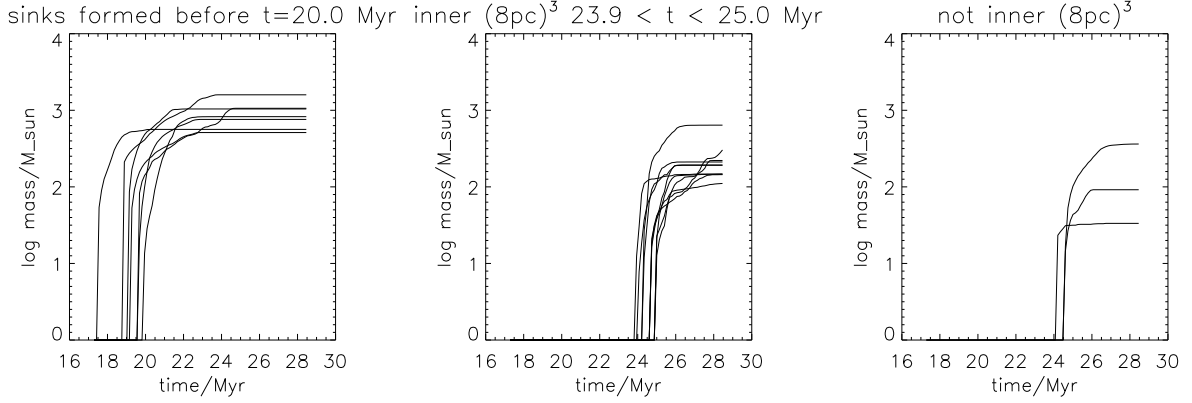


Fig. 4.— Evolution of the most massive sinks formed in the simulation up to  $t = 20$  Myr (*left panel*), the most massive sinks formed in the central 8-pc region for  $23.9 < t < 25$  Myr (*middle panel*), and those formed outside of the central 8-pc region during the same time interval (*right panel*).

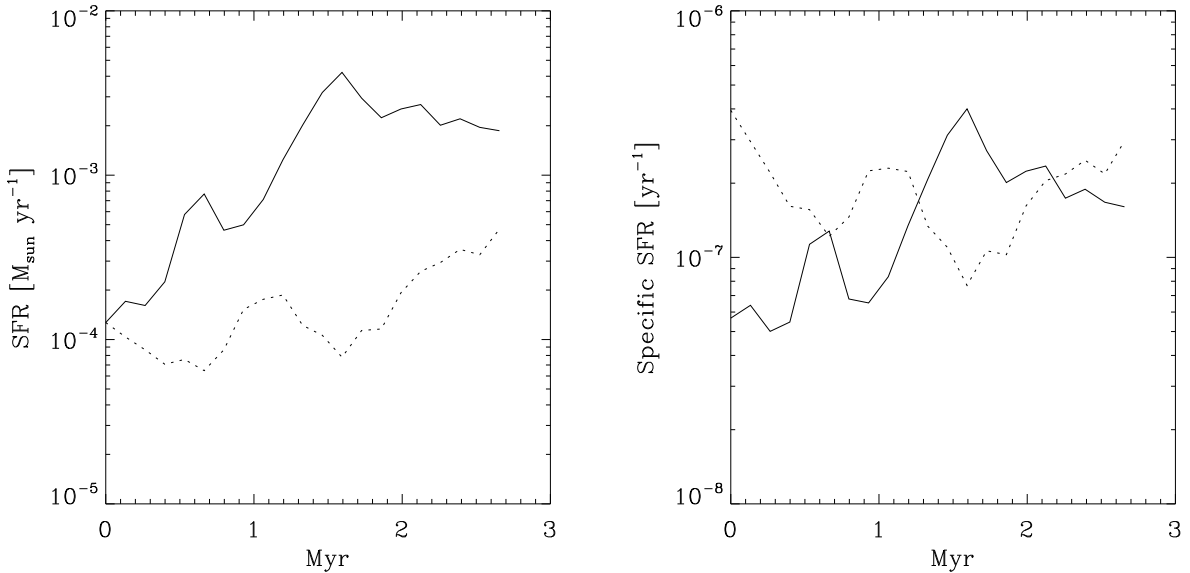


Fig. 5.— Evolution of the SiFR and the specific SiFR (*sifr*) for Cloud 1 (C1, *dotted lines*) and the Central Cloud (CC, *solid lines*).

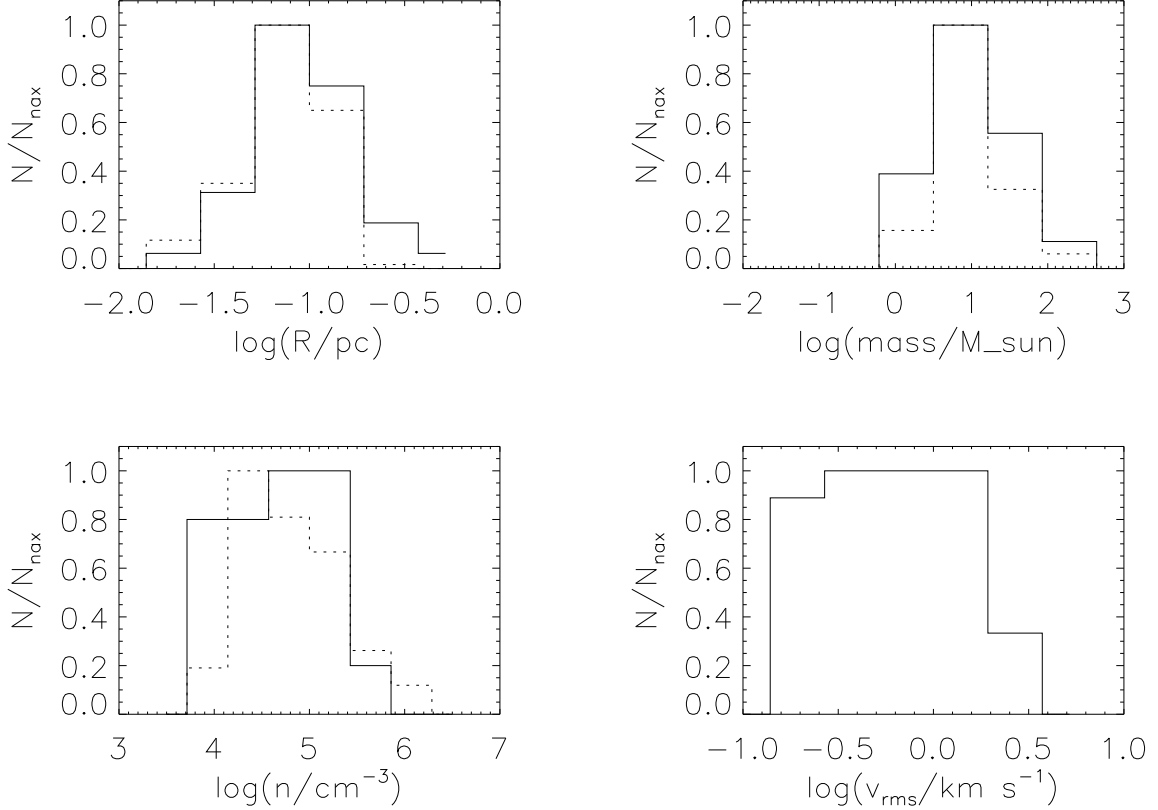


Fig. 6.— Histograms of the size (*top left*), mass (*top right*), mean density (*bottom left*) and three-dimensional velocity dispersion (*bottom right*) of the cores within the Central Cloud of the simulation (*solid lines*) at  $t = 23.9$  Myr, at which time the region acquires its most compressed state. The histograms are normalized to their peak values. *Dotted lines*: same for the core sample in Cygnus X reported by Motte et al. (2007), except for the velocity dispersion, since their observations were performed in the 1.2 mm continuum. The distributions are seen to match extremely well for size, mass and mean density.

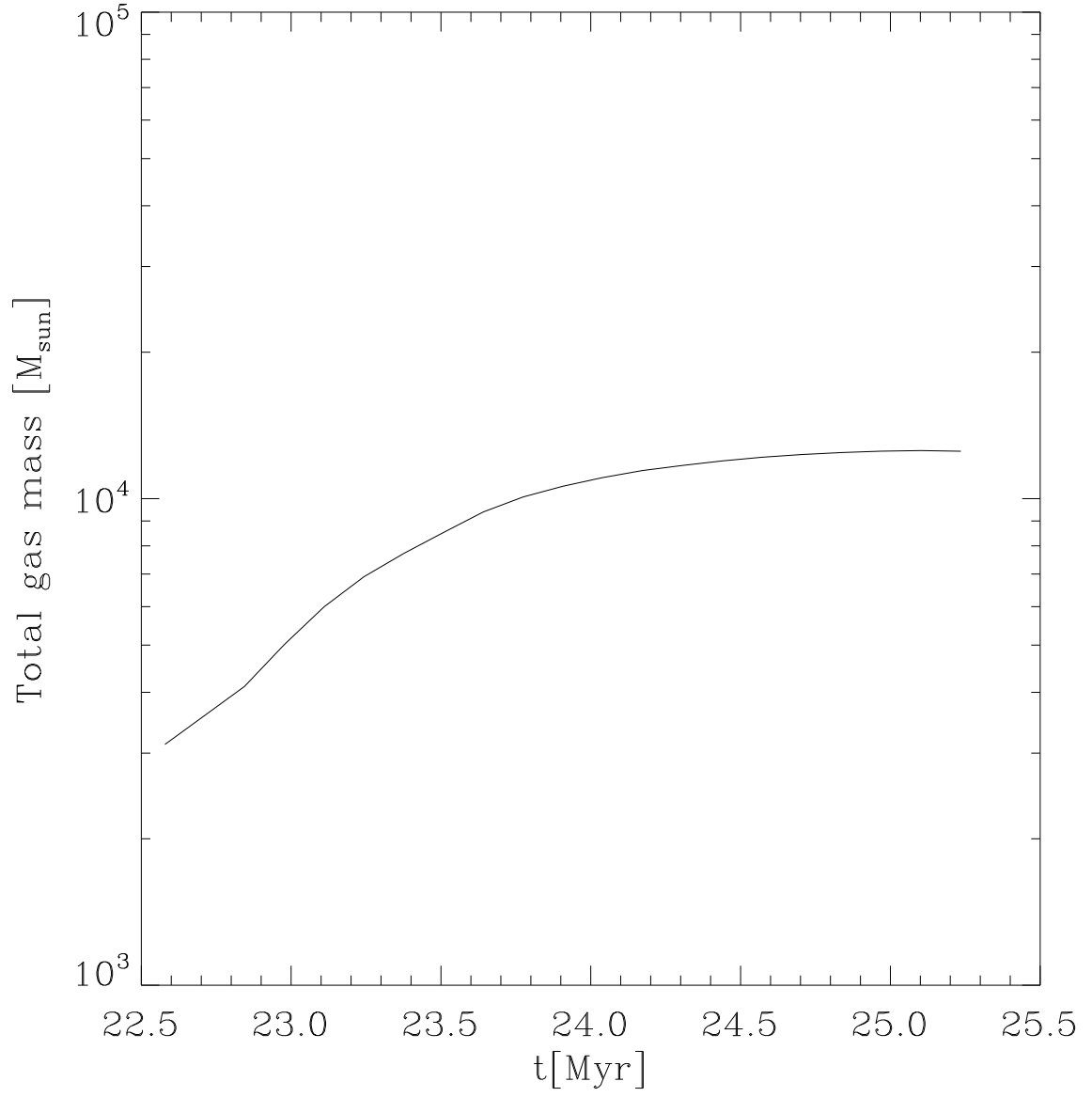


Fig. 7.— Evolution of the total gas mass in the central 8-pc box of the simulation. The total mass in this region is seen to increase from  $\sim 4 \times 10^3 M_{\odot}$  to  $\sim 1.2 \times 10^4 M_{\odot}$  in 3 Myr, corresponding to a mean accretion rate of  $2.7 \times 10^{-3} M_{\odot} \text{ yr}^{-1}$ .

## REFERENCES

- Audit, E. & Hennebelle, P. 2005, *A&A* 433, 1
- Ballesteros-Paredes, J., Hartmann, L. & Vázquez-Semadeni, E. 1999b, *ApJ* 527, 285
- Ballesteros-Paredes, J., Klessen, R. S., & Vázquez-Semadeni, E. 2003, *ApJ*, 592, 188
- Ballesteros-Paredes, J., Klessen, R. S., Mac Low, M.-M., & Vazquez-Semadeni, E. 2007, *Protostars and Planets V*, 63
- Ballesteros-Paredes, J., Vázquez-Semadeni, E., & Scalo, J. 1999a, *ApJ*, 515, 286
- Bally, J., Stark, A. A., Wilson, R. W., & Langer, W. D. 1987, *ApJ*, 312, L45
- Banerjee, R., Vázquez-Semadeni, E., Hennebelle, P., & Klessen, R. S. 2009, *MNRAS*, 398, 1082
- Bate, M. R., Bonnell, I. A., & Bromm, V. 2003, *MNRAS* 336, 705
- Beuther, H., Churchwell, E. B., McKee, C. F., Tan, J. C. 2007, in *Protostars and Planets V*, eds. B. Reipurth, D. Jewitt, and K. Keil (Tucson: University of Arizona Press), 165
- Bigiel, F., Leroy, A., Walter, F., Brinks, E., de Blok, W. J. G., Madore, B., & Thornley, M. D. 2008, *AJ*, 136, 2846
- Brunt, C. M. 2003, *ApJ*, 583, 280
- Burkert, A., & Hartmann, L. 2004, *ApJ*, 616, 288
- Caselli, P., Benson, P.J., Myers, P.C., & Tafalla, M. 2002, *ApJ*, 572, 238
- Dale, J. E., Bonnell, I. A., Clarke, C. J., & Bate, M. R. 2005, *MNRAS*, 358, 291

- Dale, J. E., & Bonnell, I. A. 2008, MNRAS, 391, 2
- Elmegreen, B. G. 1983, MNRAS, 203, 1011
- Elmegreen, B. G. 2000, ApJ, 530, 277
- Elmegreen, B. G. 2007, ApJ, 668, 1064
- Elmegreen, B. G. & Lada, C. J. 1977, ApJ, 214, 725
- Evans, N. J., et al. 2009, ApJS, 181, 321
- Faustini, F., Molinari, S., Testi, L., & Brand, J. 2009, A&A, 503, 801
- Federrath, C., Klessen, R. S., & Schmidt, W. 2008, ApJ, 688, L79
- Federrath, C., Duval, J., Klessen, R. S., Schmidt, W., & Mac Low, M.-M., 2009, A&A, submitted (arXiv:0905.1060)
- Field, G., Blackman, E. G., Keto, E. R. 2008, MNRAS, 385, 181
- Franco, J. Shore, S. N., & Tenorio-Tagle, G. 1994, ApJ 436, 795
- Frisch, U. 1995, Turbulence. The legacy of A.N. Kolmogorov (Cambridge: Cambridge University Press)
- Galván-Madrid, R., Keto, E., Zhang, Q., Kurtz, S., Rodríguez, L. F., & Ho, P. T. P. 2009, ApJ, submitted (arXiv:0910.2270)
- Garay, G. & Lizano, S. 1999, PASP, 111, 1049
- Goldreich, P., & Kwan, J. 1974, ApJ 189, 441
- Genzel, R., Reid, M. J., Moran, J. M., & Downes, D. 1981, ApJ, 244, 884
- Hartmann, L., Ballesteros-Paredes, J., & Bergin, E. A. 2001, ApJ, 562, 852

- Hartmann, L. & Burkert, A. 2007, *ApJ*, 654, 988
- Hatchell, J., Fuller, G. A., Richer, J. S., Harries, T. J., & Ladd, E. F. 2007, *A&A*, 468, 1009
- Heitsch, F., Burkert, A., Hartmann, L., Slyz, A. D. & Devriendt, J. E. G. 2005, *ApJ* 633,  
L113
- Heitsch, F., Hartmann, L., Slyz, A., Devriendt, J., & Burkert, A. 2008, *ApJ*, 674, 316
- Heitsch, F., Slyz, A., Devriendt, J., Hartmann, L., & Burkert, A. 2006, *ApJ*, 648, 1052
- Heitsch, F., Mac Low, M. M., & Klessen, R. S. 2001, *ApJ*, 547, 280
- Hennebelle, P. & Audit, E. 2007, *A&A*, 465, 431
- Hennebelle, P. & Pérault, M. 1999, *A&A* 351, 309
- Heyer, M. H., & Brunt, C. 2007, *IAU Symposium*, 237, 9
- Hillenbrand, L. A. 1997, *AJ*, 113, 1733
- Hillenbrand, L. A., & Carpenter, J. M. 2000, *ApJ*, 540, 236
- Hoyle, F. 1953, *ApJ*, 118, 513
- Hunter, J. H., Jr., & Fleck, R. C., Jr. 1982, *ApJ*, 256, 505
- Ikeda, N., Sunada, K., & Kitamura, Y. 2007, *ApJ*, 665, 1194
- Jappsen, A.-K., Klessen, R. S., Larson, R. B., Li, Y., and Mac Low, M.-M. 2005, *A&A* 435,  
611
- Jijina, J., Myers, P.C., and Adams, F.C. 1999, *ApJS*, 125, 161
- Kirk, H., Johnstone, D., & Di Francesco, J. 2006, *ApJ*, 646, 1009

- Klessen, R. S. 2001, *ApJ*, 556, 837
- Klessen, R. S., Ballesteros-Paredes, J., Vázquez-Semadeni, E., and Durán-Rojas, C. 2005, *ApJ*, 620, 786
- Klessen, R. S., & Burkert, A. 2000, *ApJS*, 128, 287
- Klessen, R. S., & Burkert, A. 2001, *ApJ*, 549, 386
- Klessen, R. S., Heitsch, F., & MacLow, M. M. 2000, *ApJ*, 535, 887
- Koyama, H. & Inutsuka, S.-I. 2002, *ApJ*, 564, L97
- Krumholz, M. R., Matzner, C. D., McKee, C. F. 2006, *ApJ*, 653, 361
- Krumholz, M. R., & McKee, C. F. 2005, *ApJ*, 630, 250
- Krumholz, M. R., & Tan, J. C. 2007, *ApJ*, 654, 304
- Kurtz, S., Cesaroni, R., Churchwell, E., Hofner, P., Walmsley, C. M. 2000, in *Protostars and Planets IV*, eds. V. Mannings, A. P. Boss, S. S. Russell (Tucson: University of Arizona Press), 299
- Lada, C. J., & Lada, E. A. 2003, *ARAA*, 41, 57
- Larson, R. B. 1987, *Starbursts and Galaxy Evolution*, 467
- Lee, C.W., & Myers, P.C. 1999, *ApJS*, 123, 233
- Li, Z.-Y. & Nakamura, F. 2006, *ApJ*, 640, L187
- Mac Low, M.-M., & Klessen, R. S. 2004, *Reviews of Modern Physics*, 76, 125
- Matzner, C. D. 2002, *ApJ*, 566, 302
- McKee, C. F., Tan, J. C. 2003, *ApJ*, 585, 850

- McKee, C. F., & Williams, J. P. 1997, *ApJ*, 476, 144
- Morata, O., Girart, J. M., & Estalella, R. 2005, *A&A*, 435, 113
- Motte, F., Bontemps, S., Schilke, P., Schneider, N., Menten, K. M., Broguire, D. 2007, *A&A*, 476, 1243
- Newman, W.I., & Wasserman, I. 1990, *ApJ*, 354, 411
- Ossenkopf, V., & Mac Low, M.-M. 2002, *A&A*, 390, 307
- Ostriker, E. C., Stone, J. M., & Gammie, C. F. 2001, *ApJ*, 546, 980
- Palla, F., & Stahler, S. W. 1999, *ApJ*, 525, 772
- Passot, T., Vázquez-Semadeni, E., & Pouquet, A. 1995,
- Peretto, N., Hennebelle, P., André, P. 2007, *A&A*, 464, 983
- Peters, Banerjee,, R., Klessen, R.S., Mac Low, M.-M., Galvan-Madrid, R., & Keto, E.,  
submitted to *Nature*
- Price, D. 2007, *PASA*, 24, 159
- Rosas-Guevara, Y., Vázquez-Semadeni, E., Gómez, G. C., & Jappsen, A.-K. 2009, *MNRAS*,  
submitted
- Sandstrom, K. M., Peek, J. E. G., Bower, G. C., Bolatto, A. D., & Plambeck, R. L. 2007,  
*ApJ*, 667, 1161
- Springel, V., Yoshida, N., White, S. D. M. 2001, *New Astron.*, 6, 79
- Stutzki, J., & Güsten, R. 1990, *ApJ*, 356, 513.
- Tachihara, K., Onishi, T., Mizuno, A., & Fukui, Y. 2002, *A&A*, 385, 909

- Tobin, J. J., Hartmann, L., Furesz, G., Mateo, M., & Megeath, S. T. 2009, *ApJ*, 697, 1103
- Vázquez-Semadeni, E., Ballesteros-Paredes, J., & Rodríguez, L.F. 1997, *ApJ*, 474, 292
- Vázquez-Semadeni, E., González, R. F., Ballesteros-Paredes, J., Gazol, A., & Kim, J. 2008, *MNRAS*, 390, 769
- Vázquez-Semadeni, E., Gómez, G. C., Jappsen, A. K., Ballesteros-Paredes, J., González, R. F., & Klessen, R. S. 2007, *ApJ*, 657, 870 (Paper I)
- Vázquez-Semadeni, E., Kim, J., Shadmehri, M. & Ballesteros-Paredes, J. 2005, *ApJ*, 618, 344
- Vázquez-Semadeni, E., Passot, T., & Pouquet, A. 1995, *ApJ*, 441, 702
- Vázquez-Semadeni, E., Passot, T., & Pouquet, A. 1996, *ApJ*, 473, 881
- Vázquez-Semadeni, E., Ryu, D., Passot, T., González, R. F., & Gazol, A., 2006, *ApJ*, 643, 245
- Walder, R. & Folini, D. 2000 *ApSS*, 274, 343
- Whitworth, A. 1979, *MNRAS*, 186, 59
- Williams, J.P., de Geus, E.J., & Blitz, L. 1994, *ApJ*, 428, 693
- Zinnecker, H., & Yorke, H. W. 2007, *ARA&A*, 45, 481
- Zuckerman, B. & Palmer, P. 1974, *ARA&A*, 12, 279